AIAA-2002-5531

OBSERVATIONS ON CFD SIMULATION UNCERTAINTIES

Serhat Hosder*, Bernard Grossman†, Raphael T. Haftka‡, William H. Mason§, and Layne T. Watson¶

Multidisciplinary Analysis and Design (MAD) Center for Advanced Vehicles
Virginia Polytechnic Institute and State University
Blacksburg, VA 24061-0203

1. Introduction

Computational Fluid Dynamics (CFD) has gained great importance as an aero/hydrodynamic analysis and design tool in recent years. CFD simulations with different levels of fidelity, ranging from linear potential flow solvers to full Navier-Stokes codes, are widely used in the multidisciplinary design and optimization (MDO) of advanced aerospace and ocean vehicles.[1] Although low-fidelity CFD tools have low computational cost and easy implementation, the full viscous equations are needed for the simulation of complex turbulent separated flows, which occur in several practical cases such as high-angle-of attack aircraft, high-lift devices, maneuvering submarines and missiles.[2] Even for cases when there is no flow separation, the use of high-fidelity CFD simulations is desirable for obtaining higher accuracy. Due to modeling, discretization and computation errors, the results obtained from CFD simulations have a certain level of uncertainty. It is important to understand the sources of CFD simulation errors and their magnitudes in order to be able to assess the magnitude of the uncertainty in the results.

Recent results presented in the *First AIAA CFD Drag Prediction Workshop*[3,4] also depict the importance of understanding the uncertainty and its sources in CFD simulations. Many of the performance quantities of interest for the DLR-F4 wing-body configuration, such as the lift curve slope, the drag polar, or the drag rise Mach number, obtained from the CFD solutions of 18 different participants using different codes, grid types, and turbulence models showed considerable amount of scatter, which revealed the general issue of accuracy and credibility in CFD simulations.

The objective of the proposed paper is to illustrate different sources of uncertainty in CFD simulations, by careful study of an example. We will try to compare the magnitude and importance of each source of uncertainty.

To have a better understanding of the accuracy in CFD simulations, the main sources of errors and uncertainties should be identified. Oberkampf and Blottner[5] classified CFD error sources. In their classification, the error sources are grouped under four main categories: (1) physical modeling errors, (2) discretization and solution errors, (3) programming errors, and (4) computer round-off errors.

Physical modeling errors originate from the inaccuracies in the mathematical models of the physics. The errors in the partial differential equations (PDEs) describing the flow, the auxiliary (closure) physical models and the boundary conditions for all the PDEs are included in this category. Turbulence models used in viscous calculations are considered as one of the auxiliary physical models, usually the most important one. They are used for modeling the additional terms originated as the result of Reynolds averaging, which in itself is a physical model.

Oberkampf and Blottner[5] define discretization errors as the errors caused by the numerical replacement of PDEs, the auxiliary physical models and continuum boundary conditions by algebraic equations. Consistency and the stability of the discretized PDEs, spatial (grid) and temporal resolution, errors originating from the discretization of the continuum boundary conditions are listed under this category. The difference between the exact solution to the discrete equations and the approximate (or computer) solution is defined as the solution error of the discrete equations. Iterative convergence error of the steady-state or the transient flow simulations is included in this category. A similar description of the discretization errors can also be found in Roache.[6,7]

Since the terms *error* and *uncertainty* are commonly used interchangeably in many CFD studies,

*Graduate student, Department of Aerospace and Ocean Engineering, Student Member AIAA

†Professor and Department Head, Department of Aerospace and Ocean Engineering, Fellow AIAA

‡Professor, Department of Aerospace Engineering, Mechanics and Engineering Science, University of Florida, Gainsville, FL, Fellow AIAA

§Professor, Department of Aerospace and Ocean Engineering, Associate Fellow AIAA

¶Professor, Departments of Computer Science and Mathematics

it will be useful to give a definition for each. Uncertainty, itself, can be defined in many forms depending on the application field as listed in DeLaurentis and Mavris.[8] For computational simulations, Oberkampf *et al.*[9,10] described *uncertainty* as a potential deficiency in any phase or activity of modeling process that is due to the lack of knowledge, whereas *error* is defined as a recognizable deficiency in any phase or activity of modeling and simulation.

Considering these definitions, any deficiency in the physical modeling of the CFD activities can be regarded as *uncertainty* (such as uncertainty in accuracy of turbulence models, uncertainty in the geometric dimensions, uncertainty in thermophysical parameters *etc.*), whereas the deficiency associated with the discretization process can be classified as *error*.[10]

Discretization errors can be quantified by using methods like Richardson's extrapolation or grid-convergence index (GCI), a method developed by Roache[7] for uniform reporting of grid-convergence studies. However, these methods require fine grid resolution in the asymptotic range, which may be hard to achieve in the simulation of flow-fields around complex geometries. Also non-monotonic grid convergence, which may be observed in many flow simulations, prohibits or reduces the applicability of such methods. That is, it is often difficult to estimate errors in order to separate them from uncertainties. Therefore, for the rest of the paper, the term *uncertainty* will be used to describe the inaccuracy in the CFD solution variables originating from discretization, solution, or physical modeling errors.

In this paper, the results of a two-dimensional, turbulent, transonic flow in a converging-diverging channel obtained with the General Aerodynamic Simulation Program (GASP)[11] are presented. Runs were performed with different turbulence models, grid levels and flux-limiters in order to see the effect of each to the CFD simulation uncertainties. In addition to these, the contribution of the error in geometry representation to the CFD simulation uncertainties is studied through the use of a modified geometry based on the data measured in the experiments. The exit station of the diffuser is varied to determine the effect of the change of the downstream boundary location on the results.

2. Description of the Simulation Case

The test case presented in this paper is the simulation of steady, 2-D, turbulent, transonic flow in a converging-diverging channel, which is also known as the *Sajben Transonic Diffuser* in the CFD validation studies. Figure 1 shows a schematic of the two versions of the geometry used in the computations. The flow is from left to right, in the positive x-direction, and y-direction is normal to the bottom wall. All the dimensions are scaled by the throat height, h_t. The throat section, which is the minimum cross-sectional area of the channel, is located at $x/h_t = 0.0$. Both geometries have the inlet stations located at $x/h_t = -4.04$. The exit station is at $x/h_t = 8.65$ for the geometry shown at the top part of Figure 1. This is the *original* geometry used in the computations and a large portion of the results with different solution and physical modeling parameters are obtained with this version. The exit station is located at $x/h_t = 14.44$ for the other geometry shown in Figure 1. This *extended* geometry is used to study the effect of varying the downstream boundary location on the CFD simulation results. For both geometries, the bottom wall of the channel is flat and the converging-diverging section of the top wall is described by an analytical function of x/h_t defined in Bogar *et al.*[12] In addition to these two geometries, a third version of the same diffuser (the *modified-wall* geometry) has been used in the calculations. This version has the same inlet and exit locations as the original geometry, but the upper wall is described by natural cubic-splines fitted to the geometric data points that were measured in the experimental studies. Having seen the fact that the upper wall contour obtained by the analytical equation and the contour described by experimental data points are slightly different, the modified-wall geometry is used to determine the effects of geometric uncertainty on the numerical results. Despite the relatively simple geometry, the flow has a complex structure. The exit-pressure-to-inlet-total pressure ratio P_e/P_{0i} sets the strength and the location of a shock that appears downstream of the throat. In our studies, for the original and the modified-wall geometries, we term $P_e/P_{0i} = 0.72$ as the strong shock case and $P_e/P_{0i} = 0.82$ as the weak shock case. A separated flow region exists just after the shock at $P_e/P_{0i} = 0.72$. Although a nominal exit station was defined at $x/h_t = 8.65$ for the diffuser used in the experiments, the physical exit station is located at $x/h_t = 14.44$. In the experiments, P_e/P_{0i} was measured as 0.7468 and 0.8368 for the strong and the weak shock cases respectively at the physical exit location. Table 1 gives a summary of the different versions of the transonic diffuser geometry and P_e/P_{0i} ratios used in the computations. A large set of experimental data for a range of P_e/P_{0i} values is available.[12] In our study, top and bottom wall pressure values were used for the comparison of CFD results

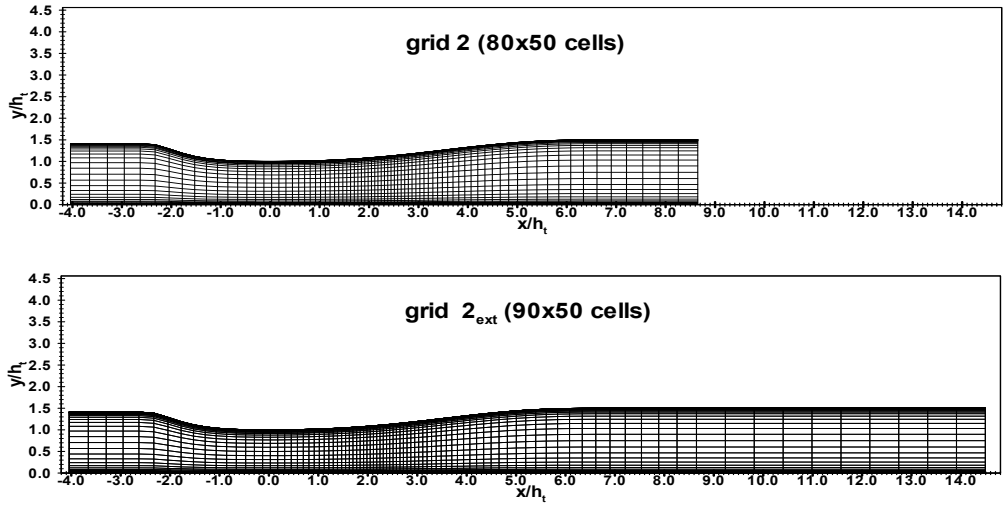

Figure 1: **Original geometry, Grid 2 (top), and extended geometry, Grid 2_{ext} (bottom) used in the computations.**

Table 1: **Different versions of the transonic diffuser geometry and P_e/P_{0i} ratios used in the computations**

Geometry	x/h_t **at the exit station**	P_e/P_{0i}
original	8.65	0.72 and 0.82
modified-wall	8.65	0.72 and 0.82
extended	14.44	0.72, 0.7468 0.82, and 0.8368

Table 2: **The size of the grids used in the computations**

Grid	x/h_t **at the exit station**	**mesh size**
g1	8.65	$41 \times 26 \times 2$
g2	8.65	$81 \times 51 \times 2$
g3	8.65	$161 \times 101 \times 2$
g4	8.65	$321 \times 201 \times 2$
g5	8.65	$641 \times 401 \times 2$
$g1_{ext}$	14.44	$46 \times 26 \times 2$
$g2_{ext}$	14.44	$91 \times 51 \times 2$
$g3_{ext}$	14.44	$181 \times 101 \times 2$
$g4_{ext}$	14.44	$361 \times 201 \times 2$
$g1_{mw}$	8.65	$41 \times 26 \times 2$
$g2_{mw}$	8.65	$81 \times 51 \times 2$
$g3_{mw}$	8.65	$161 \times 101 \times 2$

with the experiment. It should be noted that the diffuser geometry used in the experiments has suction slots placed at $x/h_t = 9.8$ on the bottom and the side walls to limit the growth of the boundary layer. The existence of these slots can affect the accuracy of the quantitative comparison between the experiment and the computation at the downstream locations.

GASP is a three-dimensional, finite-volume, Reynolds-averaged Navier-Stokes code, which is capable of solving steady-state and time-dependent problems. For this problem, the inviscid fluxes were calculated by upwind-biased 3^{rd}-order spatially accurate Roe flux scheme. The minimum modulus (Min-Mod) and Van Albada's flux limiters were used in order to prevent non-physical oscillations in the solution. All the viscous terms were included in the solution and two turbulence models, Spalart-Allmaras (Sp-Al) and k-ω (Wilcox, 1998 version), were used for modeling the viscous terms.

The iterative convergence of each solution is examined by monitoring the overall residual, which is the sum (over all the cells in the computational domain) of the L2 norm of all the governing equations solved in each cell. In addition to this overall residual information, the individual residual of each equation and some output quantities are also monitored.

In the simulations, five different grids were used for the original geometry: Grid 1 (g1), Grid 2 (g2), Grid 3 (g3), Grid 4 (g4), and Grid 5 (g5). The finest mesh is grid 5 and the other grids are obtained by reducing the number of divisions by a factor of 2 in both x and y-directions at each consecutive level (grid halving). Grid 5 is used only for the case with Sp-Al turbulence model, Min-Mod limiter, and $P_e/P_{0i} = 0.72$. Four grid levels were used for the extended geometry: Grid 1_{ext} ($g1_{ext}$), Grid 2_{ext}, ($g2_{ext}$), Grid 3_{ext} ($g3_{ext}$), and Grid 4_{ext} ($g4_{ext}$). The grids of the extended geometry and the grids generated for the original geometry are

essentially the same between the inlet station and $x/h_t = 8.65$. For the modified-wall geometry, three grid levels were used: Grid 1_{mw} ($g1_{mw}$), Grid 2_{mw} ($g2_{mw}$), and Grid 3_{mw} ($g3_{mw}$). All the grids have the same mesh distribution in the y-direction at each level. The size of the grids used in the computations are given in Table 2. Grid 2 (top) and Grid 2_{ext} (bottom) are shown in Figure 1. In order to resolve the flow gradients due to viscosity, the grid points were clustered in the y-direction near the top and the bottom walls. In wall bounded turbulent flows, it is important to have sufficient number of grid points in the wall region, especially in the laminar sublayer, for the resolution of the near wall velocity profile, when turbulence models without wall-functions are used. A measure of grid spacing near the wall can be obtained by examining the y^+ values defined as

$$y^+ = \frac{y\sqrt{\tau_w/\rho}}{\nu}, \tag{1}$$

where y is the distance from the wall, τ_w, the wall shear stress, ρ, the density of the fluid, and ν, the kinematic viscosity. In turbulent boundary layers, a y^+ value between 7 and 10 is considered as the edge of the laminar sublayer. General CFD practice has been to have several mesh points in the laminar sublayer with the first mesh point at $y^+ = O(1)$. In our study, the maximum value of y^+ values for Grid 2 and Grid 3 at the first cell center locations from the bottom wall were found to be 0.53 and 0.26 respectively. The grid points were also stretched in the x-direction to increase the grid resolution in the vicinity of the shock wave. The center of the clustering in the x-direction was located at $x/ht = 2.24$. At each grid level, except the first one, the initial conditions were obtained by interpolating the primitive variable values of the previous grid solution to the new cell locations. This method, known as *grid sequencing*, was used to reduce the number of iterations required to converge to a steady state solution at finer mesh levels.

It should be noted that grid levels like g5, g4, and $g4_{ext}$ are highly refined, beyond what is normally used for such two-dimensional problems. A single solution on Grid 4 required approximately 363 hours of total node CPU time on an SGI Origin2000 with 6 processors, when the L2 norm of the overall residual was allowed to drop 5 orders of magnitude. If we consider a three-dimensional case, with the addition of another dimension to the problem, Grid 2 would usually be regarded as a fine grid, whereas Grid 3 and Grid 4 would generally not be used.

3. Results and Discussion

For the transonic flow in the converging-diverging channel, the uncertainty of the CFD simulations are investigated by examining the nozzle efficiency (n_{eff}) as a global output quantity obtained at different P_e/P_{0i} ratios with different grids, flux limiters (Min-Mod and Van Albada), and turbulence models (Sp-Al and k-ω). n_{eff} is defined as

$$n_{eff} = \frac{H_{0i} - H_e}{H_{0i} - H_{es}}, \tag{2}$$

where H_{0i} is total enthalpy at the inlet, H_e, the enthalpy at the exit, and H_{es}, the exit enthalpy at the state that would be reached by isentropic expansion to the actual pressure at the exit. Since the enthalpy distribution at the exit was not uniform, H_e and H_{es} were obtained by integrating the cell-averaged enthalpy values across the exit plane. Besides n_{eff}, wall pressure values from the CFD simulations are compared with experimental data. In addition to the visual assessment of the graphs, the comparison with the experiment is also performed quantitatively by introducing a measure of the error between the experiment and the curve representing the CFD results, *the orthogonal distance error*

$$E_n = \frac{\sum_{i=1}^{N_{exp}} d_i}{N_{exp}}, \tag{3}$$

where

$$d_i = min_{x_{inlet} \le x \le x_{exit}} \left\{ \sqrt{(x - x_i)^2 + (P_c(x) - P_{exp}(x_i))^2} \right\}. \tag{4}$$

In equations (3) and (4), d_i represents the orthogonal distance between the i^{th} experimental point and the $P_c(x)$ curve (the wall pressure obtained from the CFD calculations), P_{exp} is the experimental wall pressure value, and N_{exp} is the number of experimental data points used. Pressure values are scaled by P_{0i} and the x values are scaled by the length of the channel.

In the transonic diffuser study, the uncertainty in the CFD simulation results has been studied in terms of five contributions: (1) the iterative convergence error, (2) the discretization error, (3) error in geometry representation, (4) the turbulence model, and (5) changing the downstream boundary location. In particular, (1) and (2) contribute to the numerical uncertainty, which is the subject of verification process; (3), (4), and (5) contribute to the physical modeling uncertainty, which is the concern of the validation process.

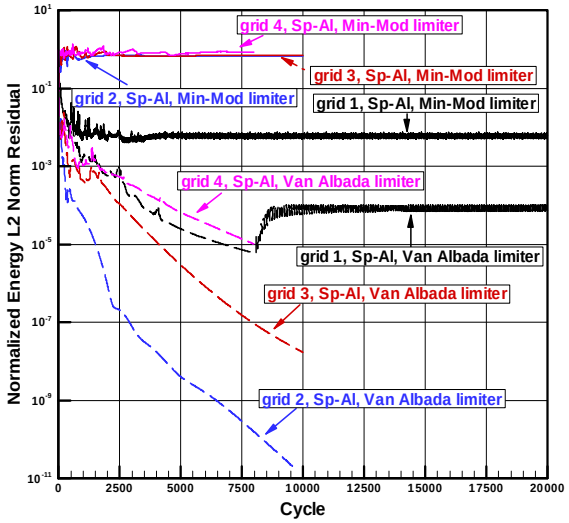

Figure 2: **Normalized L2 Norm residual of the energy equation for the case with Sp-Al turbulence model, Van Albada, and Min-Mod limiters at $P_e/P_{0i} = 0.72$ obtained with the original geometry. Normalization is done with the initial value of the residual.**

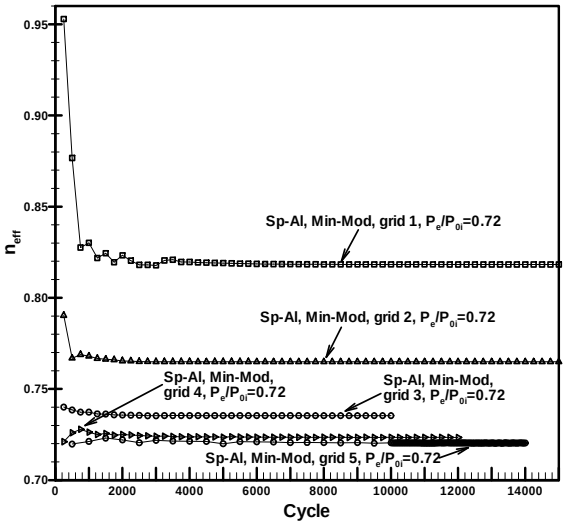

Figure 3: **Convergence history of the n_{eff} at different grid levels for the Sp-Al, Min-Mod, strong shock case obtained with the original geometry. (n_{eff} values are monitored at every 50 cycles starting from the iteration number 10000 for grid 5)**

3.1. The Iterative Convergence Error

The convergence of each case to a steady-state solution has been examined by using different L2 norm residuals and the n_{eff} results. The overall residual and the residual of each equation were monitored at every iteration, whereas the n_{eff} results were checked at certain iteration numbers. Figure 2 shows the convergence history of the L2 norm residual of the energy equation for the strong shock case obtained with the Sp-Al turbulence model and the original geometry. The convergence history of the residual, normalized by its initial value, is presented for both limiters and the grid levels g1, g2, g3, and g4. By examining this figure, it can be seen that the main parameter that affects the residual convergence of a solution is the flux-limiter. With the Min-Mod limiter, the residuals of Grid g2, g3, and g4 do not reach even one order of magnitude reduction while the same grid levels show much better residual convergence when the Van Albada limiter is used. For example, the residual of Grid 3 was reduced more than seven orders of magnitude when 10000 cycles were run with the Van Albada limiter. The same convergence behavior of the Min-Mod and the Van Albada limiter was observed for the residual of the other equations and the weak shock case. It was also seen that the case with the k-ω turbulence model exhibited the same behavior for Min-Mod and Van Albada limiters at both shock conditions.

Although the use of Min-Mod limiter causes poor L2 norm residual convergence, this does not seem to effect the final results, such as the wall pressure values or the nozzle efficiencies. Figure 3 shows the convergence history of the n_{eff} at different grid levels for the Sp-Al, Min-Mod, strong shock case obtained with the original geometry. The convergence can be seen qualitatively at all grid levels for this scale of n_{eff} axis. However, at a smaller scale, small oscillations have been observed in n_{eff} results of grids g4 and g5 starting from the iteration number 10000. The amplitude of the oscillations (the fluctuating component of the n_{eff}) were on the order of 10^{-4} after the iteration number 13000 for g5. As will be seen in the next section, the magnitude of the discretization error is much higher compared to the order of the iterative convergence error, especially in the coarser grid levels.

Although a steady-state solution is sought for each case, the physical problem itself may have some unsteady characteristics, such as the oscillation of the shock wave, which is a common phenomena observed in the transonic flows. Hsieh and Coakley[13] studied unsteady nature of the shock in the Sajben Diffuser geometry by changing the exit location. They used a physical time step of 2.77×10^{-6} seconds to resolve the time-dependent shock oscillations and wall pressures. In this study, time-dependent runs were performed with grid levels g2 and g3 by using a physical time step of 10^{-2} seconds and no change in n_{eff} values, thus no unsteady effects were observed. Therefore, it may be more appropriate to consider the output variables such as the n_{eff} or the wall pressures

obtained in this study from the steady-state CFD runs as the mean time-averaged values of the corresponding quantities.

3.2. The Discretization Error

In order to investigate the contribution of the discretization error to the uncertainty in CFD simulation results, we study the Sp-Al and k-ω cases separately. For each case with a different turbulence model, grid level and the flux-limiter affect the magnitude of the discretization error. Grid level determines the spatial resolution, and the limiter is part of the discretization scheme which reduces the spatial accuracy of the method to first order in the vicinity of shock waves.

A qualitative assessment of the discretization error in nozzle efficiency results obtained with the original geometry can be made by examining Figure 4. For each turbulence model, the relative uncertainty between the strong shock results of Grid 2 and Grid 4 is significant. The largest value of this difference is observed for the Sp-Al case with the Min-Mod limiter. For the weak shock case, the difference between each grid level is not as big as that of the strong shock case when the results obtained with the Sp-Al turbulence model are compared. The weak shock results in Figure 4 also show that the k-ω turbulence model is slightly better than the Sp-Al in terms of the discretization error for this pressure ratio. The non-monotonic behavior of the k-ω results can be seen for the strong shock as the mesh is refined, whereas the same turbulence model show monotonic convergence for the weak shock cases. Sp-Al turbulence model exhibit monotonic convergence in both shock conditions.

In order to estimate the magnitude of the discretization error at each grid level for the cases that show monotonic convergence, Richardson's extrapolation technique has been used. This method is based on the assumption that f_k, a local or global output variable obtained at grid level k, can be represented by

$$f_k = f_{exact} + \alpha h^p + O(h^{p+1}), \tag{5}$$

where h is a measure of grid spacing, p, the order of the method, and α, the p^{th} order error coefficient. It should be noted that equation 5 will be valid when f is smooth and in the asymptotic grid convergence range. In most cases, the *observed* order of spatial accuracy is different than the nominal (theoretical) order of the numerical method due to the factors such as the existence of the discontinuities in the solution domain, boundary condition implementation, flux-limiters, *etc.* Therefore, the observed value of p should be determined and be used in the calculations required for approximating f_{exact} and the discretization error. The calculation of the approximate value of the observed order of accuracy needs the solutions from three grid levels, and the estimate of the f_{exact} value requires two grid levels. The details of the calculations are given in Appendix A. Table 3 summarizes the discretization error in n_{eff} results obtained with the original geometry. It should be noted that the cases presented in this table exhibit monotonic convergence with the refinement of the mesh size. For each case with a different turbulence model, limiter, and P_e/P_{0i}, the approximation to the exact value of n_{eff} is denoted by $(n_{eff})_{exact}$ and the discretization error at a grid level k is calculated by

$$error(\%) = \left| \frac{(n_{eff})_k - (n_{eff})_{exact}}{(n_{eff})_{exact}} \times 100 \right|. \tag{6}$$

When grid level g2 results are compared, the Sp-Al, Min-Mod, and $P_e/P_{0i} = 0.72$ case has the highest discretization error (6.97%), while the smallest error (1.45%) is obtained with k-ω turbulence model at $P_e/P_{0i} = 0.82$. As also seen in Figure 4, the weak shock results of Table 3 show that the k-ω turbulence model gives lower errors than the Sp-Al model does at each grid level, when the cases with the same limiters are compared. In general, the uncertainty due to the discretization error is bigger for the cases with strong shock compared to the weak shock results at each grid level. This indicates the fact that the flow structure has significant effect on the discretization error.

The difference in n_{eff} values due to the choice of the limiter can be seen in the results of Grid 1 and Grid 2 for the strong shock case and Grid 1 for the weak shock case. The maximum difference between the Min-Mod limiter and Van Albada limiter occurs on Grid 1 with Sp-Al model. The relative uncertainty due to the choice of the limiter is more significant for the strong shock case. For both pressure ratios, the results obtained with different limiters have almost the same value, when Grid 3 and Grid 4 are used, which would hardly be the case in practice due their computational expense.

Figure 5 again shows the significance of the discretization uncertainty between each grid level. In this Figure, the noisy behavior of n_{eff} results obtained with Grid 1 can be seen for both turbulence models. The order of the noise error is much smaller than the discretization error between each grid level, however this can be a significant source of uncertainty if the results of grid 1 are used in a gradient-based optimization.

In Table 3, the observed order of accuracy p, which is also used in the $(n_{eff})_{exact}$ calculations (See Ap-

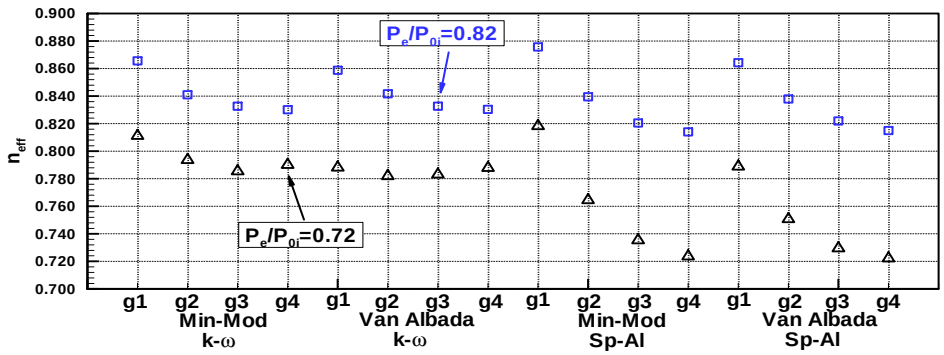

Figure 4: n_{eff} **obtained at different grid levels with the original geometry, Sp-Al and** k-ω **turbulence models, Min-Mod and Van Albada limiters.**

Table 3: **Discretization error results obtained with the original geometry**

turbulence model	**limiter**	P_e/P_{0i}	p	$(n_{eff})_{exact}$	**grid level**	**discretization error** (%)
Sp-Al	Van Albada	0.72	1.528	0.71830	g1	9.820
					g2	4.505
					g3	1.562
					g4	0.542
Sp-Al	Min-Mod	0.72	1.322	0.71950	g1	14.298
					g2	6.790
					g3	2.716
					g4	1.086
Sp-Al	Van Albada	0.82	1.198	0.80958	g1	6.761
					g2	3.507
					g3	1.528
					g4	0.666
Sp-Al	Min-Mod	0.82	1.578	0.81086	g1	8.005
					g2	3.539
					g3	1.185
					g4	0.397
k-ω	Van Albada	0.82	1.980	0.82962	g1	3.514
					g2	1.459
					g3	0.370
					g4	0.094
k-ω	Min-Mod	0.82	1.656	0.82889	g1	4.432
					g2	1.452
					g3	0.461
					g4	0.146

pendix A), has been estimated by using the n_{eff} values from grid levels g2, g3, and g4 for each case. The approximate value of the $(n_{eff})_{exact}$ has been calculated by using the n_{eff} values obtained at the grid levels g3 and g4. However, it has been seen that the values of both $(n_{eff})_{exact}$ and p depend on the grid levels used in the approximations. In Table 4, the discretization error for the Sp-Al, Min-Mod, strong shock case are presented at each grid level, including g5. The first row of this table gives the p value calculated with the results of grid g2, g3, and g4, and the $(n_{eff})_{exact}$ value obtained by using the results of grids g3 and g4. In the second row, the p value is approximated by using the grid levels g3, g4, and g5, and the $(n_{eff})_{exact}$ value is estimated by using the results from grid levels g4 and g5. The difference in p is

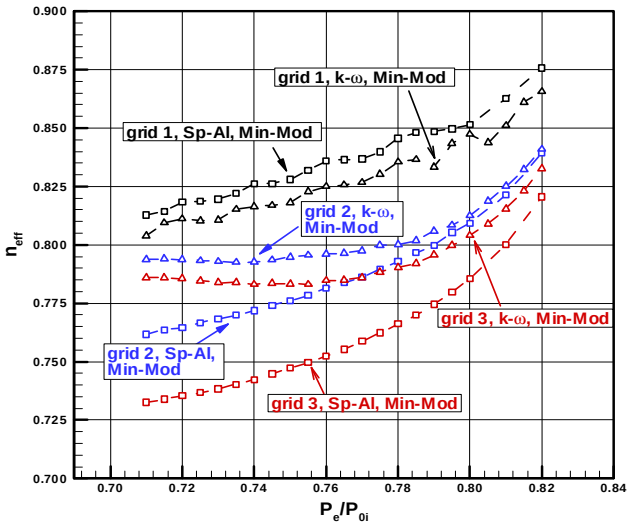

Figure 5: n_{eff} **vs.** P_e/P_{0i} **for different grids obtained with the original geometry, Sp-Al and** k-ω **turbulence models, and the Min-Mod limiter.**

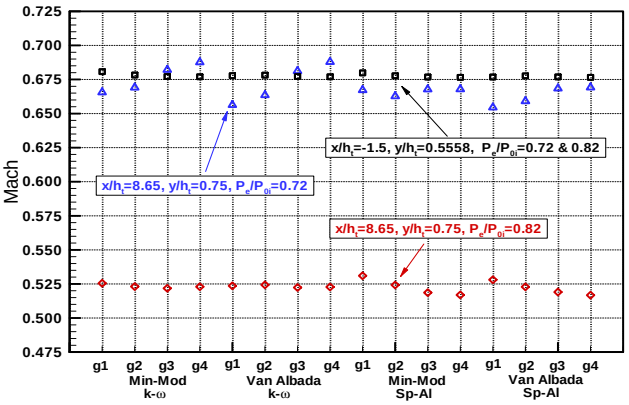

Figure 6: **Mach number values at the upstream of the shock** ($x/h_t = -1.5$)**, and downstream of the shock** ($x/h_t = 8.65$**, the exit plane) for different grids obtained with the original geometry, Sp-Al and** k-ω **turbulence models, Min-Mod and Van Albada limiters. The values of** y/h_t **correspond to the mid points of the local channel heights.**

significant between each case, however the $(n_{eff})_{exact}$ values are very close. The discretization error at grid level g5 is less than 1% in both cases.

Table 4: **Discretization errors calculated by using the results of different grid levels for the case with the original geometry, Sp-Al turbulence model, and the Min-Mod limiter.**

grid levels used	p	$(n_{eff})_{exact}$	grid level	error (%)
for p: g2, g3, and g4 *for* $(n_{eff})_{exact}$*:* g3 and g4	1.322	0.71590	g1	14.298
			g2	6.790
			g3	2.716
			g4	1.086
			g5	0.634
for p: g3, g4, and g5 *for* $(n_{eff})_{exact}$*:* g4 and g5	1.849	0.71921	g1	13.774
			g2	6.300
			g3	2.245
			g4	0.623
			g5	0.173

When we look at Mach number values at two points in the original geometry; one, upstream of the shock ($x/h_t = -1.5$) and the other, downstream of the shock ($x/h_t = 8.65$, the exit plane), both of which are located at the mid point of the local channel heights (Figure 6), we see the convergence of Mach number upstream of the shock for all the cases. However, for the strong shock case, the lack of convergence downstream of the shock at all grid levels with the k-ω model can be observed. For the Sp-Al case, we see the convergence only at Grid levels 3 and 4. For the weak shock case, downstream of the shock, the convergence at all grid levels with the k-ω model is also seen. At this pressure ratio, Sp-Al model results do not seem to converge, although the difference between each grid level is small. These results may again indicate the effect of the complex flow structure downstream of the shock, especially the separated flow region seen in the strong shock case, on the grid convergence.

3.3. Error in the Geometry Representation

The contribution of the error in geometry representation to the CFD simulation uncertainties is studied by comparing the results of the modified-wall and the original geometry obtained with the same turbulence model, limiter, and the grid level. Figure 7 gives the % error distribution in y/h_t (difference from the analytical value) for the upper wall of the modified-wall geometry at the data points measured in the experiments. Natural cubic-splines are fit to these data points to obtain the upper wall contour. The maximum error is approximately %7 and observed upstream of the throat, at $x/h_t = -1.95$. Starting from $x/h_t = 1.2$, the error is approximately constant with an average value of %0.9. The difference between the upper wall contours of the original and the modified-wall geometry in the vicinity of the throat location is shown in Figure 8. The flow becomes supersonic just after the throat and is very sensitive to the geometric irregularities for both $P_e/P_{0i} = 0.72$ and 0.82. From the top wall pressure distributions shown in Figures 9 and 10, a local expansion/compression

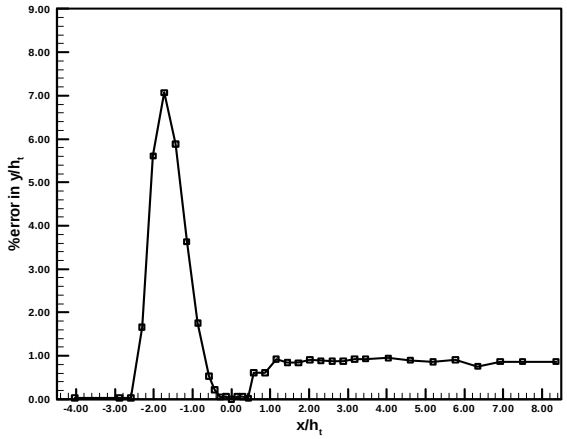

Figure 7: **Error distribution in y/h_t for the upper wall of the modified-wall geometry at the data points measured in the experiments.**

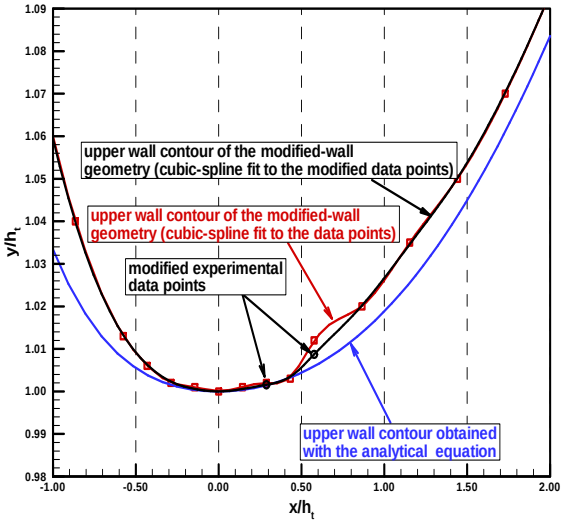

Figure 8: **Upper wall contours of the original and the modified-wall geometry in the vicinity of the throat location.**

can be seen around $x/h_t = 0.5$ with the modified-wall geometry. This is due the local bumps created by two experimental data points, the *third* and the $fifth$ one from the throat (Figure 8). Since either of the wall pressure results obtained with the original geometry or the experimental values do not have this local expansion/compression, the values of these problematic points may contain some measurement error. The locations of these two points were modified by moving them in the negative y-direction halfway between their original value and the analytical equation value obtained at the corresponding x/h_t locations. These modified locations are shown with black circles in Figure 8. The wall pressure results of the geometry with the modified experimental points (Figures 9 and 10) show that local expansion/compression region seems to be smoothed, although not totally removed. One important observation that can be made from the same figures is the improvement of the match between the CFD results and the experiment upstream of the throat when the modified-wall geometry is used. Above results suggest that the main source of the discrepancy between the CFD results of the original geometry and the experiment upstream of the shock is the error in the geometry representation. Since the viscous effects are important only in a very thin boundary layer near the wall region where there is no flow separation, contribution of the Sp-Al or the k-ω turbulence model to the overall uncertainty is very small upstream of the shock for both $P_e/P_{0i} = 0.72$ and 0.82. Downstream of the shock, wall pressure results obtained with the same turbulence model and the limiter are approximately the same regardless of the geometry used. This may imply that the difference between the experiment and the CFD results downstream of the shock is more likely due to the turbulence models when the finest grid levels are used to minimize the contribution of the discretization error.

The quantitative comparison of CFD simulation results with the experiment can be achieved by considering different measures of error. In the transonic diffuser case, the orthogonal distance error, E_n is used to approximate the difference between the wall pressure values obtained from the numerical simulations and the experimental data. E_n was evaluated separately in two regions: upstream of the experimental shock location (UESL) and downstream of the experimental shock location (DESL). The calculations were made by using equations 3 and 4. The parameters used in these equations for UESL and DESL are given in Appendix B. Table 5 lists the top wall $\hat{E_n}$ values obtained for UESL with the original geometry, different grids, turbulence models, and the flux-limiters. Table 6 gives DESL results. In these tables, $\hat{E_n}$ values were obtained by scaling E_n as

$$\hat{E_n} = \frac{E_n}{(E_n)_{max}} \times 100, \qquad (7)$$

where $(E_n)_{max}$ is the maximum E_n value calculated DESL at the strong shock case with Grid 4, Min-Mod limiter, and k-ω turbulence model. It can be seen from Table 5 that the results obtained with the Sp-Al and the k-ω turbulence models are very close, especially for the weak shock case, when the values at the grid level g4 are compared. For each P_e/P_{0i}, the small difference between the results of each turbulence model at the finest mesh level originate from

Table 5: **Top wall $\hat{E_n}$ values calculated upstream of the experimental shock location (UESL) for each case obtained with the original geometry.**

P_e/P_{0i}	Grid	Sp-Al, Min-Mod	Sp-Al, Van Albada	k-ω, Min-Mod	k-ω, Van Albada
0.72	g1	25.6	26.5	27.3	28.2
0.72	g2	23.5	24.0	26.1	25.8
0.72	g3	23.9	24.0	26.3	26.2
0.72	g4	25.8	23.8	27.3	27.1
0.82	g1	27.3	29.3	28.9	31.1
0.82	g2	27.1	27.5	28.0	28.4
0.82	g3	27.7	27.8	28.4	28.5
0.82	g4	27.6	27.6	28.2	28.2

Table 6: **Top wall $\hat{E_n}$ values calculated downstream of the experimental shock location (DESL) for each case obtained with the original geometry.**

P_e/P_{0i}	Grid	Sp-Al, Min-Mod	Sp-Al, Van Albada	k-ω, Min-Mod	k-ω, Van Albada
0.72	g1	81.2	64.4	85.6	74.6
0.72	g2	52.3	48.9	89.9	83.7
0.72	g3	35.0	34.5	90.1	89.2
0.72	g4	27.8	27.9	100.0	97.8
0.82	g1	27.1	21.4	14.6	14.6
0.82	g2	11.3	10.9	14.6	14.3
0.82	g3	17.7	16.9	12.9	13.3
0.82	g4	21.2	20.8	10.8	10.7

the difference in the shock locations obtained from the CFD calculations. This again shows that a big fraction of the uncertainty observed UESL in the wall pressure values originate from the uncertainty in the geometry representation. The difference in $\hat{E_n}$ between each grid level for each turbulence model and P_e/P_{0i} is very small indicating that the wall pressure distributions UESL obtained at each grid level are approximately the same. In other words, grid convergence is achieved upstream of the shock and the discretization error in wall pressure values at each grid level is very small.

3.4. Turbulence models

In order to approximate the contribution of the turbulence models to the CFD simulation uncertainties in the transonic diffuser case, the $\hat{E_n}$ values calculated for the top wall pressure distributions DESL (Table 6) at grid level g4 for each P_e/P_{0i} are examined. By considering the results of the finest mesh level, contribution of the discretization error is tried to be minimized, although it is difficult to isolate the numerical errors completely from the physical modeling uncertainties, especially for the strong shock case.

The Sp-Al turbulence model is more accurate than the k-ω model for the strong shock case. In fact, the difference is significant with k-ω giving the highest error of all the cases, which is bigger than the Sp-Al error by a factor of 3.6. With the Sp-Al model, the orthogonal distance error gets smaller as the mesh is refined, while the k-ω model gives the biggest error value at grid level g4. This shows that the most accurate results are not always obtained at the finest mesh level. The numerical errors and the physical modeling uncertainties may cancel each other, and the closest results to the experiment can be obtained at intermediate grid levels. When compared with the error values presented in Table 5, the uncertainty of k-ω turbulence model is 3.7 times bigger than the error due geometric uncertainty for the strong shock case. On the other hand, the uncertainty of Sp-Al model has approximately the same magnitude as the geometric uncertainty.

As opposed to the strong shock case, k-ω turbulence model gives more accurate wall pressure distributions than the Sp-Al model when the weak shock results of grid g4 are compared (Table 6). The orthogonal distance error of Sp-Al is twice as big as that of the k-ω model. The minimum error for the Sp-

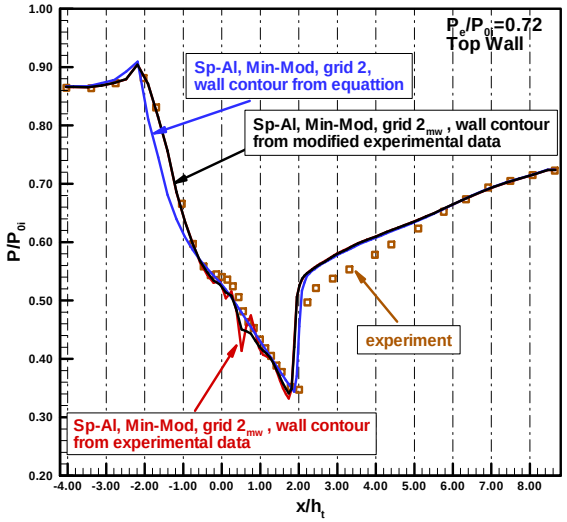

Figure 9: **Top wall pressure distributions obtained with the original and the modified-wall geometry for the strong shock case (Sp-Al model, Min-Mod limiter, and grids g3 and g3_{mw} are used).**

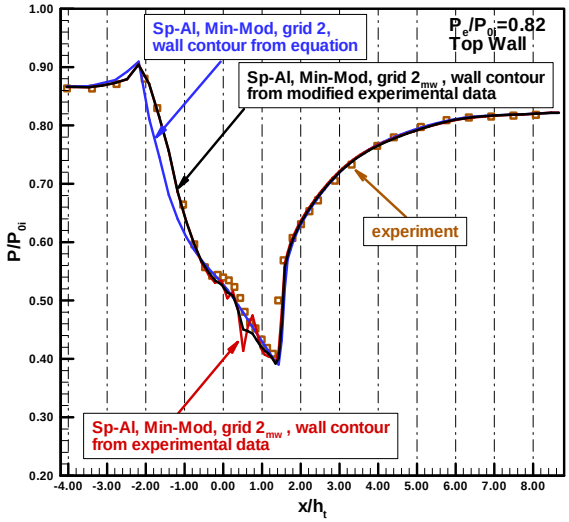

Figure 10: **Top wall pressure distributions obtained with the original and the modified-wall geometry for the weak shock case (Sp-Al model, Min-Mod limiter, and grids g3 and g3_{mw} are used).**

Al model is obtained at grid level g2, while the wall pressure distributions of the k-ω model get closer to the experimental distribution as the mesh is refined. The error due to the geometric uncertainty is bigger than the uncertainty of the k-ω model by a factor of 2.6. The uncertainty of the Sp-Al model is slightly smaller than the geometric uncertainty. The strong and the weak shock results show that for each flow condition, the highest accuracy in terms of the wall pressure distributions are obtained with a different turbulence model, although Sp-Al model gives reasonable results for both shock conditions.

The orthogonal distance error results can also be used to approximate the relative uncertainty at each grid level due to the selection of the turbulence model. For the strong shock case with flow separation, it can be seen that the relative uncertainty originating from the selection of turbulence models is much bigger than the uncertainty due to the discretization errors. In table 5, the difference in $\hat{E}_n$ between Sp-Al and k-ω model is 72% of $(E_n)_{max}$ at Grid level 4. This is much bigger than the difference in $\hat{E}_n$ between Grid 2 and 4 obtained with each turbulence model.

It should be noted that the experimental data have also uncertainty originating from many factors such as geometric irregularities, difference between the actual P_e/P_{0i} and its intended value, measurement errors, heat transfer to the fluid, *etc.* We have discussed the error due to geometric irregularities in the previous section. In a way, this error in geometry representation can also be regarded as part of uncertainty in the experimental data. By evaluating the orthogonal distance error in two separate regions, DESL and UESL, we tried to approximate the contribution of the geometric uncertainty to the CFD results obtained with the original geometry. However, experimental wall pressure values may still have a certain level of uncertainty associated with the rest of the factors.

3.5 Changing the Downstream Boundary Location

The effect of the downstream boundary location variation on the CFD simulation results of the transonic diffuser case has been investigated by using the extended geometry, which has the physical exit station at the same location as the geometry used in the actual experiments. For the strong shock case, the runs were performed with the Sp-Al model and two P_e/P_{0i} ratios, 0.72 and 0.7468. The second pressure ratio is the same value measured at the physical exit station of the geometry used in the experiments for the strong shock case. The results obtained with the extended geometry were compared to the results of the original geometry. Figure 11 shows the streamline patterns in the separated flow region obtained with different geometries and the P_e/P_{0i} ratios in the strong shock case. The comparison of the separation bubble size is given in Figure 12. The separation bubble obtained with the extended geometry and $P_e/P_{0i} = 0.72$ is bigger and extends more in the downstream direction compared to the other two cases. The separation bubbles obtained with the orig-

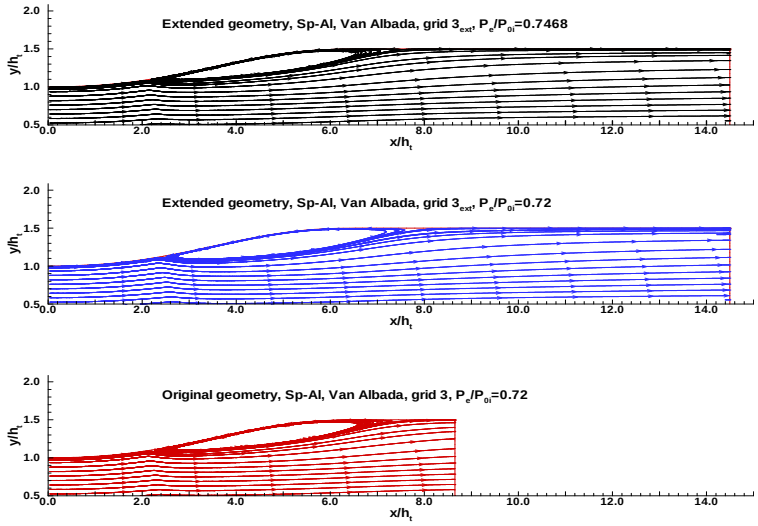

Figure 11: **Streamline patterns of the separated flow region obtained with different versions of the diffuser geometry and P_e/P_{0i} ratios at the strong shock case.**

inal geometry, $P_e/P_{0i} = 0.72$; and the extended geometry, $P_e/P_{0i} = 0.7468$ are approximately the same in size. These results are also consistent with the top wall pressure distributions given in Figure 13.

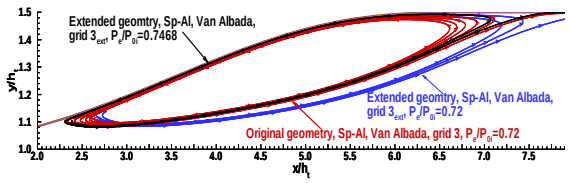

Figure 12: **Comparison of the separation bubbles obtained with different versions of the diffuser geometry and P_e/P_{0i} ratios at the strong shock case.**

With the extended geometry and $P_e/P_{0i} = 0.72$, the flow accelerates more under the separation bubble, thus the pressure is lower compared to the other cases where the separation bubbles have smaller thickness. As the exit location is moved further in the downstream, the strength of the shock and the size of the separation region increase. As the shock gets stronger, it moves downstream. On the other hand, increasing the P_e/P_{0i} reduces the strength of the shock, and moves the shock location upstream. As can bee seen from Figure 11, the separated flow region in the original geometry is close to the downstream boundary. This may be thought as one of the factors that affect the grid convergence in the strong shock case, however the discretization error analysis of the n_{eff} values obtained with the extended geometry do not show any improvement in terms of the grid convergence (Appendix D).

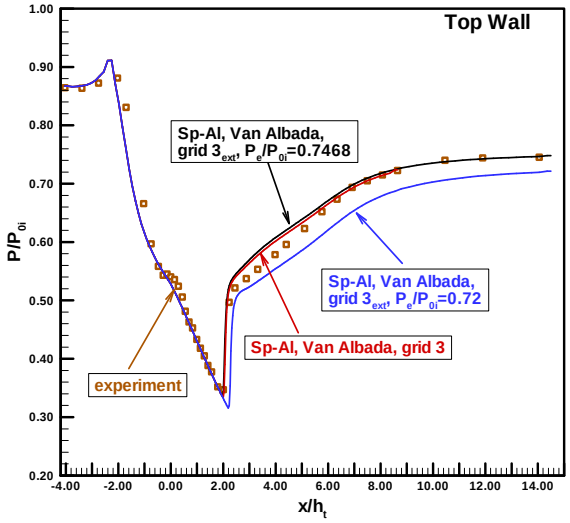

Figure 13: **Top wall pressure distributions obtained with different versions of the diffuser geometry and P_e/P_{0i} ratios for the strong shock case (Sp-Al model, Van Albada limiter, and grids g3 and g3_{ext} are used).**

4. Conclusions

Different sources of uncertainty in the CFD simulations are demonstrated by examining a 2-D, turbulent, transonic flow in a converging-diverging channel at various P_e/P_{0i} ratios by using the commercial CFD code GASP. Runs were performed with different turbulence models (Sp-Al and k-ω), grid levels, and flux-limiters (Min-Mod and Van Albada). The uncertainty in the CFD simulation results has been studied in terms of five contributions: (1) the iterative con-

vergence error, (2) the discretization error, (3) error in geometry representation, (4) the turbulence model, and (5) changing the downstream boundary location. In addition to the original geometry used in the calculations, the contribution of the error in geometry representation to the CFD simulation uncertainties is studied through the use of a modified geometry based on the data measured in the experiments. Also an extended version of the transonic diffuser is used to determine the effect of the change of the downstream boundary location on the results.

Although the use of Min-Mod limiter causes poor L2 norm residual convergence, this does not seem to effect the final results, such as the wall pressure values or the nozzle efficiencies. The order of the iterative convergence error is much less than the discretization error, especially in the coarser grid levels.

For each case with a different turbulence model, grid level and the flux-limiter affect the magnitude of the discretization error. In order to estimate the magnitude of the discretization error in nozzle efficiency results (the global output quantity) at each grid level for the cases that show monotonic convergence, the Richardson's extrapolation technique has been used. In general, the uncertainty due to the discretization error is bigger for the cases with the strong shock compared to the weak shock results at each grid level. This indicates that the flow structure has significant effect on the magnitude of the discretization error. Grid convergence is achieved upstream of the shock, whereas the lack of spatial convergence for the local quantities is observed downstream of the shock. The observed order of spatial accuracy is different than the nominal order of the scheme. The value of the observed order of accuracy depends on the grid levels used for its approximation.

The effect of the limiter on the discretization error is seen at Grid levels g1 and g2, especially for the strong shock case. For both pressure ratios, the results obtained with different limiters have almost the same value, when Grids g3 and g4 are used. However these grid levels are highly refined, and would generally not be considered in practice.

The main source of the discrepancy between wall pressure results of the CFD runs performed with the original geometry and the experiment upstream of the shock is the error in the geometry representation. The difference between the experiment and the CFD results downstream of the shock is more likely due to the turbulence models when the finest grid levels are used to minimize the contribution of the discretization error.

The strong and the weak shock results show that for each flow condition, the highest accuracy in terms of the wall pressure distributions are obtained with a different turbulence model, although Sp-Al model gives reasonable results for both shock conditions. The most accurate results are not always obtained at the finest mesh level. The numerical errors and the physical modeling uncertainties may cancel each other, and the closest results to the experiment can be obtained at intermediate grid levels. For the strong shock case with flow separation, it can be seen that the relative uncertainty originating from the selection of turbulence models is much bigger than the uncertainty due to the discretization errors.

The change of the exit location and P_e/P_{0i} ratio affect the location and the strength of the shock. For the strong shock case, the size of separation bubble is also affected by the same factors. The separated flow region in the original geometry is close to the downstream boundary. This may be thought as one of the factors that affect the grid convergence in the strong shock case, however the discretization error analysis of the n_{eff} values obtained with the extended geometry do not show any improvement in terms of the grid convergence.

Acknowledgements

This research was supported by the National Science Foundation grant DMI-9979711.

References

[1] Hosder, S., Watson, L. T., Grossman, B., Mason, W. H., Kim, H., Haftka, R. T., and Cox, S. E. Polynomial Response Surface Approximations for the Multidisciplinary Design Optimization of a High Speed Civil Transport. *Optimization and Engineering*, 2(4), 2002.

[2] Jameson, A. and Martinelli, L. Mesh Refinement and Modeling Errors in Flow Simulation. *AIAA Journal*, 36(5):676–686, May 1998.

[3] Levy, D. W., Zickuhr, T., Vassberg, J., Agrawal, S., Wahls, R. A., Pirzadeh, S., and Hemsch, M. J. Summary of Data from the First AIAA CFD Drag Prediction Workshop. *AIAA Paper 2002-0841*, January 2002.

[4] Hemsch, M. J. Statistical Analysis of CFD Solutions from the Drag Prediction Workshop. *AIAA Paper 2002-0842*, January 2002.

[5] Oberkampf, W. L. and Blottner, F. G. Issues in Computational Fluid Dynamics Code Verification and Validation. *AIAA Journal*, 36(5):687–695, May 1998.

[6] Roache, P. J. Quantification of Uncertainity in Computational Fluid Dynamics. *Annual Review of Fluid Mechanics*, 29:123–160, 1997.

[7] Roache, P. J. *Verification and Validation in Computational Science and Engineering*. Hermosa Publishers, Albuquerque, New Mexico, 1998.

[8] DeLaurentis D. A. and Mavris, D. N. Uncertainity Modeling and Management in Multidisciplinary Analysis and Synthesis. *AIAA Paper 2000-0422*, January 2000.

[9] Guide for the verification and Validation of Computational Fluid Dynamics Simulations. *AIAA Standart G-077-1998*, January 1998.

[10] Oberkampf, W. L. and Trucano, T. G. Validation Methodology in Computational Fluid Dynamics. *AIAA Paper 2000-2549*, June 2000.

[11] *GASP User Manuel*. AeroSoft, Inc., Blacksburg, Virginia, 1997.

[12] Bogar, T. J., Sajben, M., and Kroutil, J. C. Characteristic Frequencies of Transonic Diffuser Flow Oscillations. *AIAA Journal*, 21(9):1232–1240, September 1983.

[13] Hsieh T. and Coakley, T. J. Downstream Boundary Effects on the Frequency of Self-excited Oscillations in Transonic Ciffuser Flows. *AIAA Paper 87-0161*, January 1987.